Universidad de La Laguna
Escuela de Doctorado y Posgrado
Master de Astrofísica

Estructura y Evolución Estelar

Curso 2023/2024

Óscar Soler Pérez

Stellar Models

Abstract

Simple stellar models are essential to derive basic ideas of stellar structure and evolution, and can be verified against theoretical predictions and observations. In the present work a stellar model by Ekström et al. 2012 is deeply studied, comparing its results with theoretical predictions. It is checked that general scale relation behaviour is conserved, while evolutionary tracks and abundances match what is expected through the different theoretical stages of stellar evolution.

1 Introduction

The study and modelling of stellar structure is crucial to understanding the physical processes happening inside stars and causing stellar evolution. Due to the complex and immeasurable characteristics of real stars, models are essential to derive basic ideas of these celestial bodies and to obtain new insights by comparing them with observations.

This powerful tool of numerical simulation has evolved through time along with observations. Multi-object spectrography, spectropolarimetry or interferometry in large scale surveys allow to acquire data of a huge population of stars and compare the observations with those derived by stellar models, endorsing astrophysicists to comprehend and test complex models.

In the present work, the data tabulated by Ekström et al. 2012 will be analyzed and compared with the theory studied in the course imparted by Comerón 2023. The models will compare evolution for masses of 0.8, 1, 1.25, 1.5, 2, 3, 4, 5, 7, 9, 15, 25 and 40 $M_\odot$, studying central abundances (Section 3.1), positions in the Hertzsprung-Russell diagram (Section 3.2), scale relations of mass-luminosity, density and central temperature (Section 3.2), the $(\log T, \log \rho)$ plane (Section 3.3) and radius evolution (Section 3.4).

2 Methodology

The present work was executed using 13 evolutionary models of different mass, solar metallicity and no rotation from Ekström et al. 2012. The data was read, transformed and visualized through a *Python* code available here. AÑADIR CÓDIGO. Four separate tasks were executed, analyzing the evolution of different variables and comparing with theoretical expected results.

3 Results and discussion

3.1 Central H and He abundances evolution

In the first task the central hydrogen and helium abundances for stars with $M = 5M_\odot$ and $M = 9M_\odot$ were represented (see Figure 1a). The main sequence (MS), characterized by hydrogen burning in the core of the star, ends when central hydrogen abundance approaches zero (gray dotted line). The duration of the main sequence is measured as $8.9 \cdot 10^7$ years in the 5 $M_\odot$ case and $2.6 \cdot 10^7$ years in the 9 $M_\odot$ case. As expected, the main sequence lifetime is greater for less massive stars.

Figure 1b displays the time duration of the MS for all of the different masses considered in this work. It can be checked that main sequence duration decreases when increasing mass at an exponential rate

of $\tau_{MS} \propto M^{-2.2}$. In Chapter 7 of the theory studied in class [Comerón 2023], we saw by simply doing dimensional analysis that $\tau_{MS} \propto M^{-2}$. That deduction assumed $L \propto M^3$, ignoring variation of this dependence for different mass ranges. It can be seen in Figure 1b that the slope of -2.2 is an intermediate value and the real slope varies, being steepest at lower masses and getting more horizontal progressively.

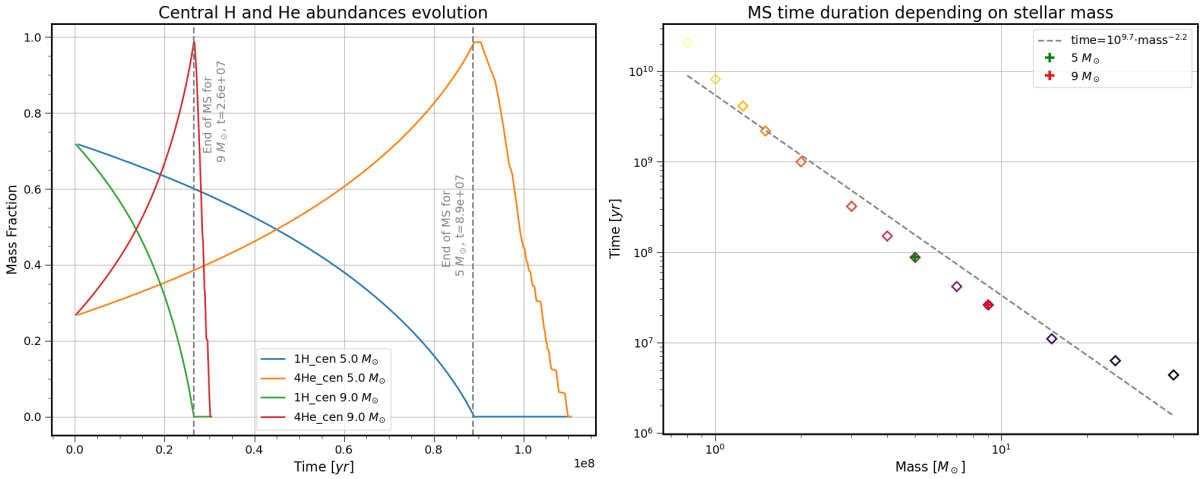

(a) Central hydrogen and helium abundances evolution with time for stars of 5 and 9 $M_\odot$. The vertical dashed lines represent the end of the main sequence (MS) for both masses.

(b) Duration of main sequence for all the different masses considered in this work. In green and red the specific masses of the previous figure. The gray dashed line represents a linear fit to the logarithmic points.

Figure 1

3.2 HR diagram and different relations for ZAMS stars

In the following part, the different evolutionary tracks were plotted in a Hertzsprung-Russell (HR) diagram, $\log(L)$ *vs* $\log(T_{eff})$, drawn in Figure 2. The different coloured lines represent the evolutionary tracks of the different masses considered, from 0.8 to 40 $M_\odot$. The dashed gray line represents the ZAMS (Zero Age Main Sequence) while the dotted gray line represents the TAMS (Terminal Age Main Sequence). The times at which each star model reaches the ZAMS (τ_{ZAMS}) and the TAMS (τ_{TAMS}) are seen in Table 1.

Mass $[M_\odot]$	0.8	1.0	1.25	1.5	2	3	4	5	7	9	15	25	40
τ_{ZAMS} $[yr]$	7.5E7	4.5E7	2.7E7	1.6E7	9.1E6	2.9E6	1.4E6	8.3E5	4.0E5	2.5E5	1.2E5	6.0E4	3.6E4
τ_{TAMS} $[yr]$	2.2E10	8.5E9	4.2E9	2.2E9	1.0E9	3.2E8	1.5E8	8.9E7	4.2E7	2.7E7	1.1E7	6.4E6	4.5E6

Table 1: Times of entry (τ_{ZAMS}) and departure (τ_{TAMS}) of the main sequence for all stellar masses considered in this work.

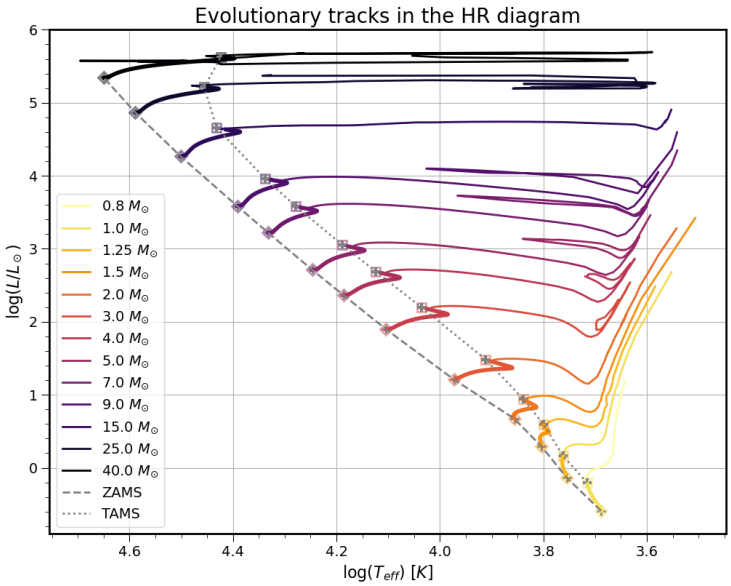

Figure 2: Evolutionary tracks of the different masses in the Hertzsprung-Russell diagram. The dashed gray line represents the ZAMS (Zero Age Main Sequence) while the dotted line represents the TAMS (Terminal Age Main Sequence).

Main sequence behaviour can specially be distinguished for stars above and below 1.5 $M_\odot$. For the most massive stars, a global cool down behaviour can be seen, with a characteristic hook towards its end. These stars burn hydrogen in their core through the CNO cycle. They will have a convective core, creating a well mixed region outside of the core. Towards the end of this core burning phase, when central hydrogen abundance is almost zero ($X \sim 0.03$), there is a Kelvin-Helmholtz contraction, in which the star keeps its luminosity constant but decreases its radius, until an outer shell of hydrogen can begin burning around the inert helium core [Comerón 2023, Chapter 8]. Through the contraction, as $L \propto R^2 T_{eff}^4$, effective temperature must increase, explaining the hook seen in the evolutionary tracks at the end of the main sequence.

For stars with mass below 1.5 $M_\odot$, their MS evolution is much more vertical, without reducing their effective temperature. They burn hydrogen through the $p-p$ chain. As their core is not convective, when the central hydrogen is already combusted, a small compression will ignite shell hydrogen burning, so the transition from core to shell burning of hydrogen is smooth [Comerón 2023, Chapter 8].

Different relations were also compared for ZAMS stars, drawing logarithmic values with respect to the logarithm of the mass of the stars. Three intervals of mass were established:

- Low masses: $M < 1.8 M_\odot$. Dominated by Kramer's opacity and burn hydrogen through $p-p$ chain.
- Intermediate masses: $1.8 M_\odot < M < 10 M_\odot$. Dominated by Kramer's opacity and burn hydrogen through the CNO cycle.
- Large masses: $M > 10 M_\odot$. Dominated by electron scattering opacity and burn hydrogen through the CNO cycle.

Figure 3a shows $\log(L/L_\odot)$ *vs* $\log(M/M_\odot)$. Theoretically and from observations, $L \propto M^\nu$, with ν a value from 2 to 5. In this work we have obtained $\nu = 4.6$ for low mass stars, 3.6 for intermediate mass and 2.5 for the most massive. Theoretically, for hot stars dominated by electron scattering opacity, $L \propto M^3$, while for lower temperature stars Kramer's opacity dominates and $L \propto M^{\frac{10n+31}{5+2n}}$ which gives $\nu \approx 5.5$ for $n = 4$ ($p-p$ chain) or $\nu \approx 5.2$ for $n = 16$ (CNO cycle) [Comerón 2023, Chapter 7]. These results are depicted in Table 2.

Regarding central density and mass relation $\log(\rho_c)$ *vs* $\log(M)$ shown in Figure 3b. From $\rho_c \propto M/R_c^3$ and $R_c \propto M^{\frac{n-1}{n+3}}$ (for stars dominated by electron scattering opacity), one can derive that $\rho_c \propto M^{\frac{-2n+6}{n+3}}$

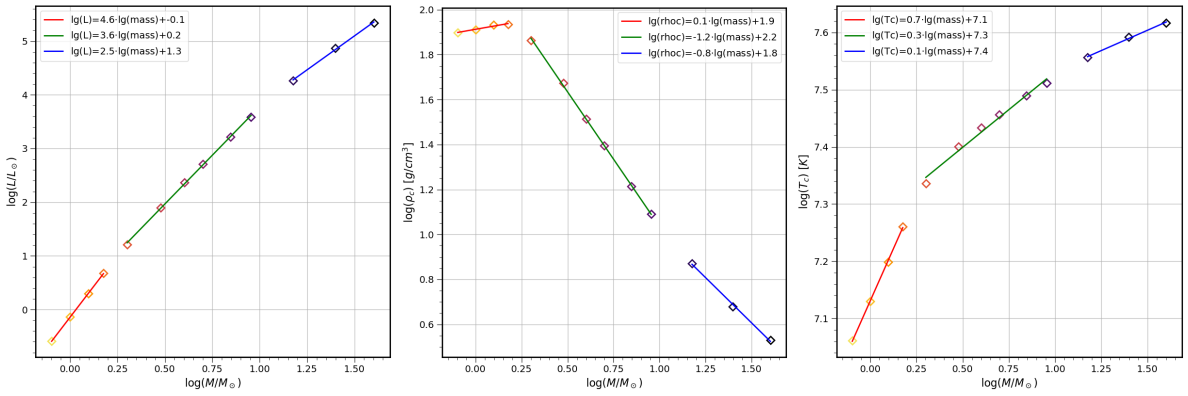

(a) $\log(L)$ *vs* $\log(M)$ (b) $\log(\rho_c)$ *vs* $\log(M)$ (c) $\log(T_c)$ *vs* $\log(M)$

Figure 3: Different mass relations for stars in the ZAMS. The linear fits performed separate the masses in three groups: low mass ($M < 1.8M_\odot$), shown in red; intermediate mass ($1.8M_\odot < M < 10M_\odot$), shown in green; and high mass ($M > 10M_\odot$), shown in blue.

[Comerón 2023, Chapter 7]. It dominates in hot stars with $n = 16$, so $\nu \approx -1.4$. For the less massive stars Kramer's opacity dominates and one uses $R_c \propto M^{\frac{2n-7}{2n+5}}$. For $n = 16$ (CNO cycle) $\nu \approx -1.0$ and for $n = 4$ ($p-p$ chain) $\nu \approx -0.8$

Figure 3c represents the central temperature and mass relation $\log(T_c)$ *vs* $\log(M)$. Using $T_c \propto M/R_c$ and $R_c \propto M^{\frac{n-1}{n+3}}$ (for stars dominated by electron scattering opacity, the massive ones), one can derive that $T_c \propto M^{\frac{4}{n+3}}$. They follow the CNO cycle so $n = 4$, leading to $\nu \approx 0.3$. For stars dominated by Kramer's opacity $R_c \propto M^{\frac{2n-7}{2n+5}}$, deriving $T_c \propto M^{\frac{12}{2n+5}}$. For $n = 16$ (CNO cycle), $\nu \approx 0.3$, while for $n = 4$ ($p-p$ chain) $\nu \approx 0.9$ [Comerón 2023, Chapter 7].

It can be said that the theoretical mass relations hold qualitatively, allowing to deduce whether the variables are inversely or directly proportional and give an idea of the rate in all cases, but are not exactly accurate in predicting the slope for the density relation and some intervals of the luminosity relation.

Mass group	C: Calculated T: Theoretical	$L \propto M^\nu$	$\rho_c \propto M^\nu$	$T_c \propto M^\nu$
Low mass	C	4.6	0.1	0.7
	T	5.5	-0.8	0.9
Intermediate mass	C	3.6	-1.2	0.3
	T	5.2	-1.0	0.3
High mass	C	2.5	-0.8	0.1
	T	3	-1.4	0.3

Table 2: Exponents obtained for the different mass relations shown in Figure 3. The rows with C represent the calculated values, while the rows with T represent the theoretical values. Expressions for theoretical values are provided in the text.

3.3 $(\log T, \log \rho)$ plane

For the models of 1, 3, 9 and 40 $M_\odot$ the $(\log T, \log \rho)$ plane is plotted in Figure 4. The ZAMS and TAMS points are specified. The areas dominated by the different equations of state of the gas are also drawn: ideal gas in gray, classic degenerate gas in red, relativistic degenerate gas in green and radiation gas in blue. The borders of these regions are given by supposing equilibrium in pressure of both type of gases:

- Between an ideal gas and a classic degenerate gas the line is obtained by $P_{ideal} = P_{class\ deg}$, and

after some manipulation:

$$\log \rho = \frac{3}{2} \log T + \frac{3}{2} \log \left(\frac{\mathcal{R}}{\mu_\odot} \frac{\mu_e^{5/3}}{10^7} \right) - 3$$

where $\mathcal{R} = 8314 \frac{\mathrm{J}}{\mathrm{K}\ kg}$ is the ideal gas constant, $\mu_\odot = 0.61$ is the mean molecular weight for solar metallicity and $\mu_e = 2$ is the mean molecular weight for a star completely devoid of hydrogen.

- Between an ideal gas and a relativistic degenerate gas $P_{ideal} = P_{rel\ deg}$, and through manipulation one obtains

$$\log \rho = 3 \log T + 3 \log \left(\frac{\mathcal{R}}{\mu_\odot} \frac{\mu_e^{4/3}}{1.24 \times 10^{10}} \right) - 3.$$

- Between a classic and a relativistic degenerate gas $P_{class\ deg} = P_{rel\ deg}$, and after some manipulation:

$$\log \rho = 3 \log \left(\frac{1.25 \times 10^{10}}{\mu_e^{4/3}} \frac{\mu_e^{5/3}}{10^7} \right) - 3.$$

- Between an ideal gas and a radiation gas $P_{ideal} = 10 P_{rad}$, and through manipulation:

$$\log \rho = 3 \log T + \log \left(\frac{4\sigma}{3c} \frac{\mu_\odot}{\mathcal{R}} \right) - 3 - 1.$$

The constant value -3 that appears in all lines is due to the conversion of units, as the density in the models is given in g/cm^3 and the calculations are performed in kg/m^3

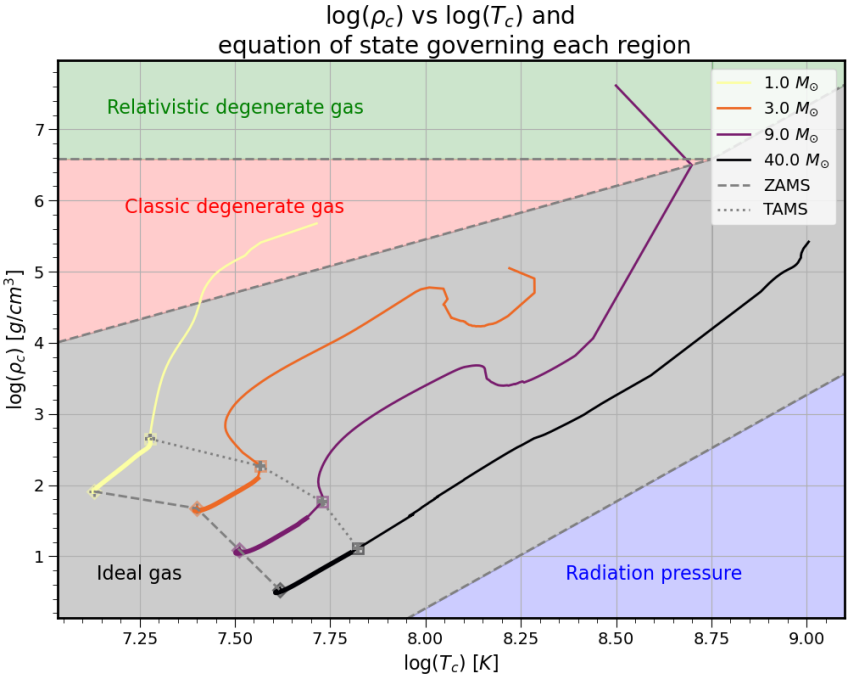

Figure 4: $(\log T, \log \rho)$ plane for models 1, 3, 9 and 40 $M_\odot$ models. The ZAMS and TAMS points are specified, and the background colors indicate the equation of state that governs each region. In gray, an ideal gas; in red, a classic degenerate gas; in green, a relativistic degenerate gas and in blue, a radiation gas.

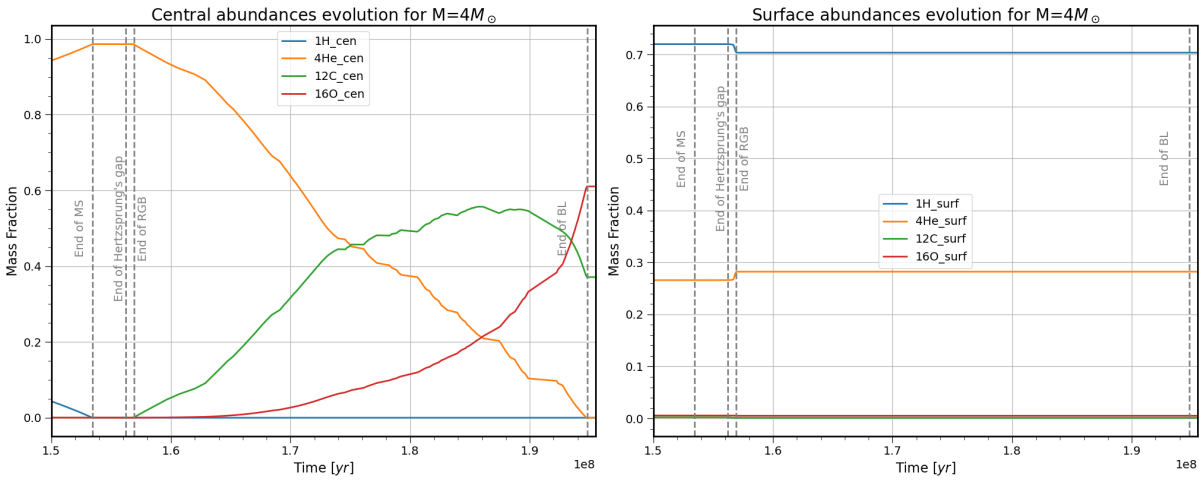

(a) Evolution of central abundances.

(b) Evolution of surface abundances.

Figure 5: Evolution of abundances of hydrogen, helium, carbon and oxygen for the model with $M = 4M_\odot$. Vertical lines indicate the end of the main sequence (MS), the Hertzsprung gap, the Red Giant Branch (RGB) and the Blue Loop (BL). The x-axis has been cropped to allow greater detail as the main sequence is much longer than other periods.

3.4 Evolution of the $M = 4M_\odot$ model

Figure 5a represents the time evolution of the central abundances of hydrogen, helium, carbon and oxygen for the case of $M = 4M_\odot$, with vertical lines indicating the end of each evolutionary phase. Figure 5b represents the time evolution of surface abundances.

- Main Sequence: it is the core hydrogen burning phase. It ends when the hydrogen in the nucleus of the star has all been consumed.
- Hertzsprung gap: empty space in the HR diagram between the main sequence and the red giant branch, present in intermediate mass stars, due to their rapid migration to a redder colour [Comerón 2023, Chapter 9]. When all the central hydrogen is exhausted, the star collapses and hydrogen shell burning begins. As the core increases its mass due to residues of helium from shell burning, it will reach the Schönberg-Chandrasekhar limit [Schönberg et al. 1942] and will become unstable and collapse until a gradient of temperature is able to counteract the collapse. At the end of this phase the star has a thin shell burning of hydrogen and it has an expanded envelope almost fully convective (see Figure 8, showing the rapid envelope expansion). It can be better identified in Figure 6 as the point with lowest luminosity of the data.
- Red giant branch: the star moves up through its Hayashi track [Hayashi 1961]. It expands and increases its luminosity to keep its effective temperature roughly constant (once again see Figure 8). Convection extends deeper, and products of hydrogen burning are dredged-up to the surface. These variations in surface composition cannot be appreciated in Figure 5a as it only represents central abundances, but are clearly detailed in Figure 5b. It can be seen that hydrogen abundance decreases as it gets dragged down by convection and combusted inside, while helium abundance increases due to the dredge-up of residues of nuclear reactions. By the end of this phase, the core is has considerably increased its temperature.
- Blue loop: helium ignition takes place. As seen in Figure 5a, helium abundance decreases while it gets burnt and carbon abundance increases rapidly as the combustion is through the 3α reaction, producing carbon nuclei. When the fraction of carbon has increased considerably the 4α reaction takes relevance, using also carbon and producing oxygen [Comerón 2023, Chapter 9]. In this process the star varies undergoes a contraction and posterior expansion (see Figure 8 showing the clear contraction and posterior expansion in the blue loop) at roughly constant temperature, increasing and decreasing its effective temperature until it ends in almost the same place where it began.

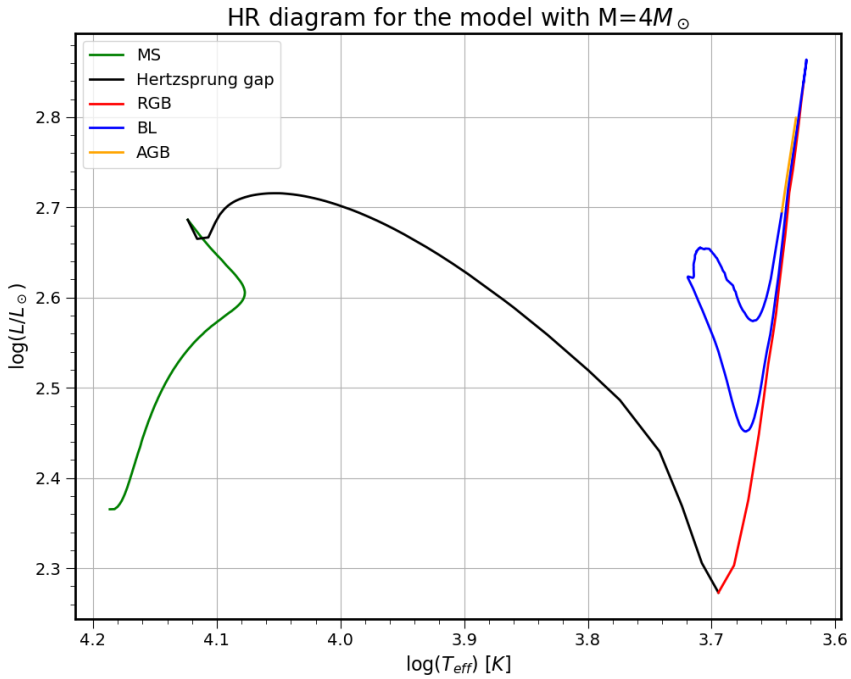

Figure 6: HR diagram for the model with $M = 4M_\odot$. The different parts of stellar evolution are represented with colours: main sequence (MS) in green, Hertzsprung gap in black, red giant branch (RGB) in red, blue loop (BL) in blue and the asymptotic giant branch (AGB) in orange.

- Asymptotic giant branch: begins as soon as helium core burning stops. In a similar fashion as when hydrogen core burning stopped, there is an inert core of residues (carbon and oxygen this time), a shell burning helium and further away another shell burning hydrogen. The model ends early in this phase, so consequences of the AGB such as thermal pulsing or more dredge-ups are not visible.

Figure 7 represents the evolution of this star in the $(\log T, \log \rho)$ plane, with the different parts of the star's evolution drawn in different colours. It can be observed that the star spends its whole life inside the ideal gas region, without getting degenerated.

Figure 8 exhibits the behaviour of the radius of the star with $M = 4M_\odot$. It is calculated using Stefan-Boltzmann's law:

$$L = 4\pi R^2 \sigma T_{eff}^4 \qquad \longrightarrow \qquad R = \sqrt{\frac{L}{4\pi\sigma T_{eff}^4}}.$$

This star begins its main sequence with $R = 2.2R_\odot$ and ends it with $4.5R_\odot$. It was seen that through the Hertzsprung gap and the red giant branch the nucleus undergoes a rapid contraction, which results in a global expansion of the envelope of the star because of the mirror principle [Comerón 2023, Chapter 9]. The expansion reaches a maximum radius of $51M_\odot$. After that, when the blue loop begins, it undergoes a global contraction (up to $25M_\odot$) and posterior expansion (up to $38M_\odot$). In the early stages of the asymptotic giant branch it keeps expanding at a high rate.

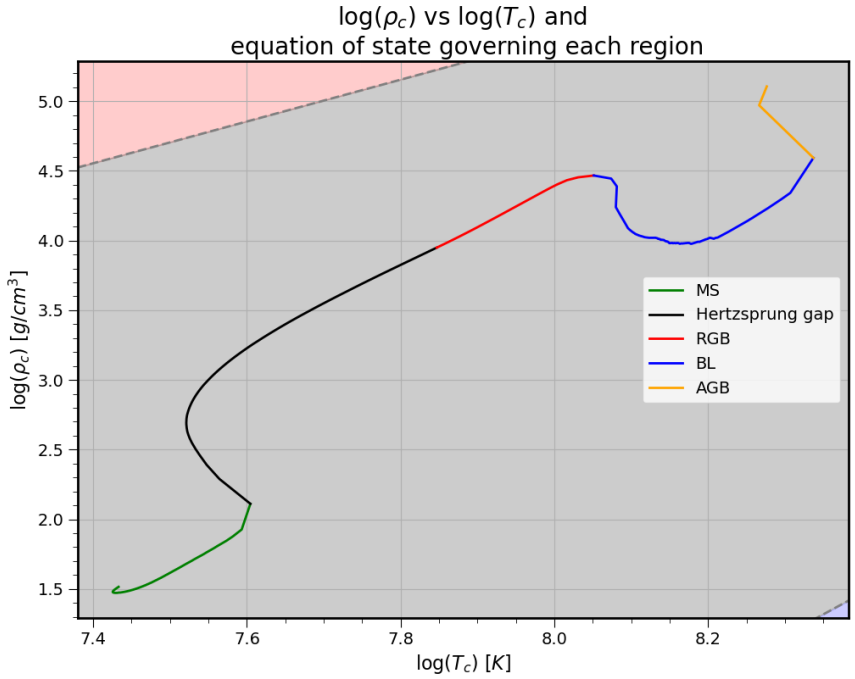

Figure 7: $(\log T, \log \rho)$ plane for model with $M = 4M_\odot$. The different parts of stellar evolution are represented with colours: main sequence (MS) in green, Hertzsprung gap in black, red giant branch (RGB) in red, blue loop (BL) in blue and the asymptotic giant branch (AGB) in orange. The gray colour of the background represents that the equation of state that governs this region is that of an ideal gas.

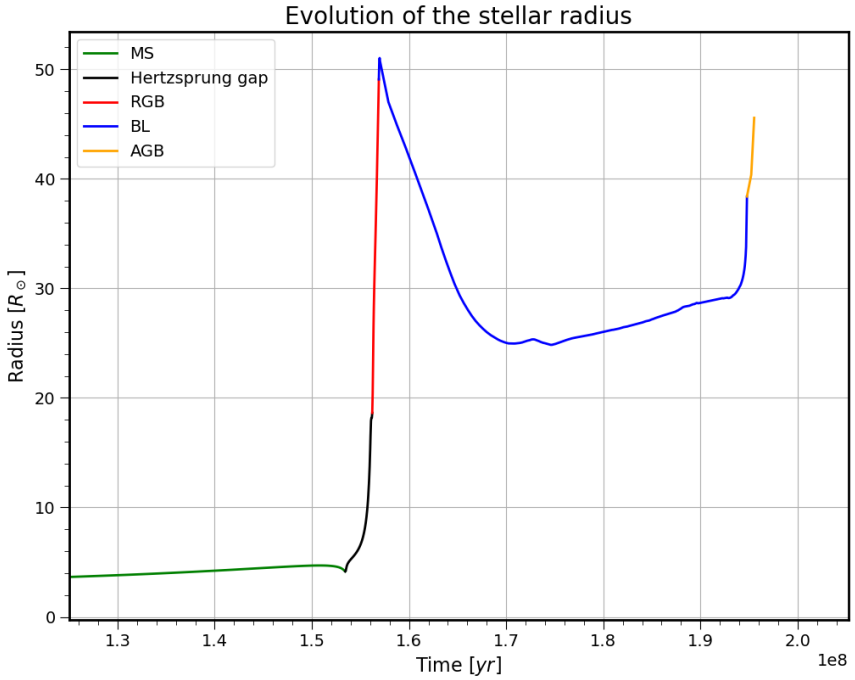

Figure 8: Evolution of the stellar radius from the end of the main sequence (green) through the Hertzsprung gap (black), the red giant branch (RGB), the blue loop (BL) and up to the asymptotic giant branch (AGB). The radius is calculated using Stefan-Boltzmann's law.

4 Conclusion

In this work an exhaustive analysis of the stellar models carried out by Ekström et al. 2012 has been carried out. It has been compared with general theory of stellar evolution, providing insights and detail in some relations that are too simple in the literature, while also allowing to appreciate the beauty of the homology relations, which concede intuition of the behaviour of these systems.

Even though exhaustive in the parameters studied, the selected models contained 42 variables out of which only 14 were used, so further work could involve learning and studying these extra parameters.

References

Comerón, S (2023). *Course notes*. Estructura y Evolución Estelar, Máster de Astrofísica, ULL.

Ekström, S et al. (Jan. 2012). "Grids of stellar models with rotation. I. Models from 0.8 to 120 $M_{\odot}$ at solar metallicity (Z = 0.014)". In: 537, A146, A146. DOI: 10.1051/0004-6361/201117751. arXiv: 1110.5049 [astro-ph.SR].

Hayashi, C (Jan. 1961). "Stellar evolution in early phases of gravitational contraction." In: 13, pp. 450–452.

Schönberg, M et al. (Sept. 1942). "On the Evolution of the Main-Sequence Stars." In: 96, p. 161. DOI: 10.1086/144444.